JOURNAL OF GEOPHYSICAL RESEARCH, VOL. 99, NO. D2, PAGES 3677-3684, FEBRUARY 20, 1994

High-resolution analysis of direct and scattered radiation in the stratosphere between 175 and 210 nm

K. Minschwaner

Advanced Study Program, National Center for Atmospheric Research, Boulder, Colorado

Abstract. Direct and scattered components of solar radiation in the stratosphere are examined at wavelengths between 175 and 210 nm. Absorption by oxygen in the Schumann-Runge system is treated exactly using temperature dependent cross sections at a spectral resolution of 0.5 cm^{-1} ($\approx$ 0.002 nm). Consistent with previous studies employing spectrally averaged cross sections, the calculated ratio of scattered to direct flux is more than a factor of 2 smaller than observed below 210 nm. The flux ratio is constrained above a minimum value at large opacities due to a twilight effect, occurring when the attenuation of scattered light from overhead paths is not as great as over the slant path of the direct beam; however, this phenomenon alone cannot account for observations. An improved description of scattering by O_2 for wavelengths below 200 nm is presented which includes effects of incoherent scattering. Use of the revised parameters for oxygen scattering does not bring the calculated flux ratios into agreement with observations, but does lead to small changes in the scattered field and O_2 photodissociation rate below 190 nm.

Introduction

A number of key photochemical reactions in the middle atmosphere are driven by solar radiation at wavelengths less than 210 nm. Absorption of radiation by O_2 in the Herzberg continuum ($\lambda < 242$ nm) and Schumann-Runge bands ($\lambda <$ 203 nm) represents the principal means for production of ozone in the stratosphere and mesosphere [*Nicolet*, 1971; *Brasseur and Solomon*, 1984]. The penetration of radiation between 190 and 210 nm governs, to a large extent, the photodissociation of several species in the stratosphere, including N_2O, NO, and chlorofluorocarbon molecules [*Froidevaux and Yung*, 1982] The actinic flux is the quantity that determines rates for photolysis in the atmosphere *Madronich* [1987], containing contributions from both the direct beam and from scattered solar radiation. Reliable estimates of rates for photodissociation are thus contingent on the accuracy to which the direct and scattered radiation fields are computed. Unfortunately, for validation purposes there are relatively few measurements of direct solar radiation below 210 nm in the stratosphere [*Frederick et al.*, 1981; *Herman and Mentall*, 1982; *Anderson and Hall*, 1983, 1986].

Herman and Mentall [1982] observed the direct solar beam and the scattered radiation from six viewing directions at 40-km altitude. The total scattered flux (integrated over 4π steradians) was estimated by logarithmic interpolation between adjacent viewing angles. The ratio of the total scattered flux to the direct flux, a quantity independent of the solar irradiance above the atmosphere, was found to be significantly larger than the value calculated by *Luther and Gelinas* [1976] for wavelengths less than about 210 nm. More recently, *Lary and Pyle* [1991] and *Kylling et al.* [1993] compared the results of their radiative transfer calculations to the observations by Herman and Mentall. They also found discrepancies below about 210 nm; computed ratios were smaller than observations by as much as a factor of 3. It was pointed out that the differences might be related to the use of spectrally averaged cross sections to approximate complex absorption features in the Schumann-Runge bands [*Herman and Mentall*, 1982; *Lary and Pyle*, 1991; *Kylling et al.*, 1993]. Another possibility may be related to the adopted cross section for molecular scattering at wavelengths less than 200 nm. It has long been recognized that molecular polarizabilities, which are related to Rayleigh and Raman scattering cross sections, may increase significantly when the frequency of incident radiation is nearly resonant with the energy required for electronic transitions [e.g., *Stone*, 1963], a situation which occurs for 20% of atmospheric scatterers (oxygen) at wavelengths below 203 nm.

The present work involves a high-resolution treatment of direct and scattered radiation for wavelengths between 175 and 210 nm. The procedures used for comparison between theory and experiment are outlined in the following section. Next, a new calculation of the molecular scattering properties of oxygen in the Schumann-Runge band region is described. The final section concludes with a discussion of the impact of these refinements on the discrepancy between theory and observations.

Paper number 93JD02988.
0148-0227/94/93JD-02988$05.00

High-Resolution Calculations

The O_2 Schumann-Runge cross sections used here are adopted from *Minschwaner et al.* [1992]. Calculations are carried out at 0.5 cm^{-1} (about 0.002 nm) intervals, providing sufficient spectral resolution to capture the narrow features of spin-split rotational lines in the Schumann-Runge bands. Cross sections for the Herzberg continuum underlying the bands are taken from the work of *Yoshino et al.* [1988]. This combination of Schumann-Runge band and Herzberg continuum cross sections has been shown to provide good agreement with cross sections measured in the laboratory over a range of temperatures and, in addition, allows for faithful reproduction of the measured attenuation of solar radiation in the stratosphere [*Minschwaner et al.*, 1992, 1993]. Results presented in this section employ cross sections for molecular scattering according to the formulae presented by *Nicolet* [1984]. Mie scattering by aerosols will be neglected as the focus here is on comparison with observations at 40-km altitude, well above the height of the main Junge layer located near 20 km [*Rosen et al.*, 1975]. This issue is addressed further in section 4. Cross sections for ozone follow the recommendations of *DeMore et al.* [1992]. Ozone makes an important contribution to atmospheric opacity in spectral regions between Schumann-Runge lines; near 200 nm, ozone absorption accounts for about 30% of the total optical depth at 40 km. Finally, vertical profiles for pressure, temperature, and ozone amount are adopted from the table provided by *Kylling et al.* [1993], as measured or inferred by *Herman and Mentall* [1982].

The algorithm for molecular scattering is patterned after the model described by *Meier et al.* [1982]. The method employs a source function, S, to solve the integral equation of transfer

$$S(\tau,t,\mu) = S_o(\tau,t,\mu) + \frac{1}{2}\int_{\tau(0)}^{\tau(\infty)} S(\tau',t',\mu)E_1\left(|(\tau+t)-(\tau'+t')|\right)d\tau' \quad (1)$$

where S is the (normalized) specific intensity integrated over all angles, assuming isotropic scattering and a plane-parallel atmosphere.

The scattering optical depth, denoted here by τ, is determined by

$$\tau(z) = \sigma_M N_M(z) \quad (2)$$

where σ_M is the cross section for molecular scattering and N_M is the vertical column abundance of air molecules above altitude z. The optical depth for molecular absorption, t, must be evaluated differently because absorption cross sections are temperature dependent:

$$t(z) = \int_z^\infty [\sigma_{O2}(z')n_{O2}(z') + \sigma_{O3}(z')n_{O3}(z')]\,dz' \quad (3)$$

The quantities σ_{O2} and σ_{O3} are the absorption cross sections for oxygen and ozone, respectively; n_{O2} and n_{O3} denote corresponding number densities.

The source function given by equation (1) represents a normalized, monochromatic, actinic flux. The product of the source function and the solar irradiance at the top of the atmosphere provides a measure of the radiative energy input to a volume element at a particular wavelength. The first term on the right hand side of equation (1) gives the contribution from the direct solar beam,

$$S_o = \exp\left[-\frac{\tau+t}{\mu}\right] \quad (4)$$

where μ is the cosine of the solar zenith angle. The second term on the right side of equation (1) accounts for scattered radiation integrated over all angles and altitudes. The angular integration is contained in the exponential integral function, $E_1(\tau,t,\tau',t')$. Note that reflection from the ground can be neglected in this analysis because absorption optical depths at the surface are very large for this spectral region.

The direct solar flux is displayed in Figure 1 for an altitude of 40 km and a solar zenith angle of 42°, corresponding to conditions of the experiment by *Herman and Mentall* [1982]. Solar fluxes at the top of the atmosphere are specified according to measurements from SUSIM [*VanHoosier et al.*, 1988]. As indicated in Figure 1, the spectral dependence of the direct flux is dominated by absorption features in the Schumann-Runge bands. Figure 1 also shows results for the spectrally degraded flux, obtained by convolution with a triangular function of halfwidth 0.3 nm. This passband was chosen to match the spectral resolution of the direct flux measurements by Herman and Mentall, which are also displayed in Figure 1. The low-resolution calculations are generally about 10 to 20% higher than the measurements, a result most likely related to an offset in values for the solar flux at the top of the atmosphere.

The scattered flux shown in Figure 2 also bears the signature of the Schumann-Runge bands when viewed at high resolution. The low-resolution fluxes displayed in Figure

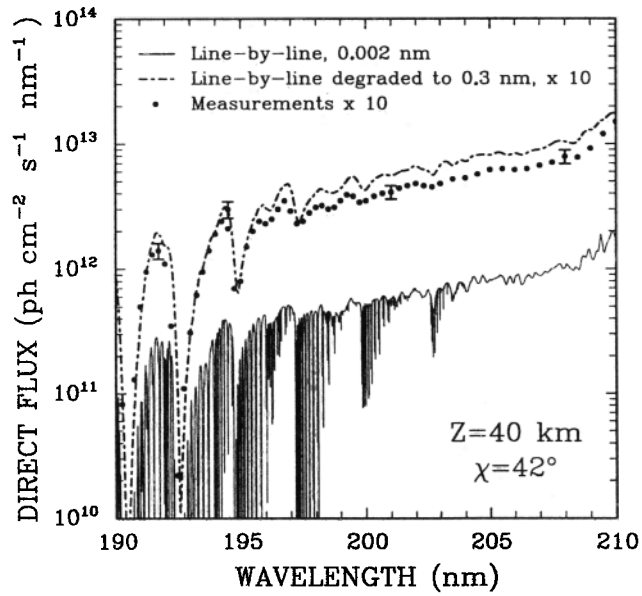

Figure 1. The direct solar flux calculated at a spectral resolution of about 0.002 nm (solid curve), and degraded to 0.3-nm resolution (dash-dot curve). Also shown are the measurements by *Herman and Mentall* [1982] (circles). The error bars indicate the magnitude of uncertainty in the measurements. The low-resolution fluxes have been multiplied by a factor of 10 for clarity.

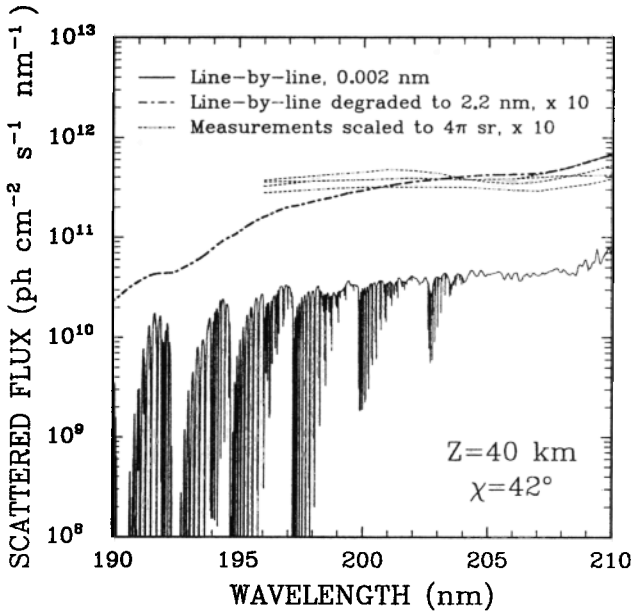

Figure 2. The scattered flux integrated over all angles at 0.002-nm spectral resolution (solid curve) and at 2.2-nm resolution (dash-dot curve). Radiances measured by *Herman and Mentall* [1982] (dotted curves) are scaled to represent 4π steradians. Low-resolution fluxes have been multiplied by 10.

2 are spectrally degraded to correspond to the resolution (2.2 nm halfwidth) of the scattered radiances measured by *Herman and Mentall* [1982]. Figure 2 shows the measurements obtained from four viewing directions (zenith angles of 48°, 93°, 138°, and 180°), all scaled to represent 4π sr. The observed scattered radiation is nearly isotropic below 210 nm; the scaled results thus provide an indication of the range of values expected for the angularly integrated, scattered radiation field. Here we find that the calculations severely underestimate observed fluxes below about 200 nm.

The ratio of scattered to direct flux is given by

$$R(\tau, t, \mu) = \frac{\frac{1}{2}\int S(\tau', t', \mu) E_1\left(|(\tau + t) - (\tau' + t')|\right) d\tau'}{S_o} \tag{5}$$

Note that the solar flux does not appear in the expression for the flux ratio, which depends only on the scattering and absorption properties within the atmosphere. Calculated values of R are presented in Figure 3. At high resolution, the behavior of R follows the Schumann-Runge band structure because the scattered flux decreases more rapidly than the direct flux for increasing levels of absorption. However, ratios near the centers of strong absorption lines display an inverted pattern: at large opacities the scattered flux does not fall off as rapidly as the direct flux. This effect defines a minimum ratio which occurs near $R = 0.02$ for the conditions shown in Figure 3.

The minimum in R can be interpreted in terms of the "twilight effect" discussed by *Davies* [1993], where attenuation of the scattered flux originating from regions overhead is not as great as the reduction in direct flux over a slant path. Consider, for example, an approximate treatment where $\sigma_{O2} \gg \sigma_M$ and $S = \exp[-t'/\mu]$. Under these conditions, extinction of the direct flux is dominated by molecular absorption and the source function is driven by the direct beam radiation, corresponding to the case of single scattering. Furthermore, assume that the scattered field originates from a thin (scattering optical thickness $\Delta\tau'$) layer located overhead. Neglecting the temperature dependence of O_2 cross sections, the ratio of scattered to direct flux is then

$$R(t, \mu) = \frac{\frac{1}{2}\exp\left[-N'\sigma_{O2}/\mu\right] E_1\left([N - N']\sigma_{O2}\right)\Delta\tau'}{\exp\left[-N\sigma_{O2}/\mu\right]} \tag{6}$$

where N is the vertical column of O_2 at optical depth t and N' corresponds to the O_2 column above the scattering layer. Letting $\eta = N - N'$, equation (6) can be written

$$R = \frac{1}{2}\exp\left[\frac{\eta\sigma_{O2}}{\mu}\right] E_1(\eta\sigma_{O2})\Delta\tau' \tag{7}$$

Differentiating equation (7) with respect to σ_{O2} and setting the result equal to zero, we have

$$E_1(\eta\sigma_{O2}) - \frac{\mu}{\eta\sigma_{O2}}\exp[-\eta\sigma_{O2}] = 0 \tag{8}$$

This defines an approximate criteria for a minimum in R. At a solar zenith angle of 42°, $\mu = 0.74$, and equation (8) can be solved numerically to obtain $\eta\sigma_{O2} = 2.6$. If the scattering layer is located near 45 km, then $\eta \simeq 6.5 \times 10^{21}$ cm^{-2} and $\sigma_{O2} \simeq 4 \times 10^{-22}$ cm^2, in agreement with the magnitude of the cross section where R exhibits a minimum value in Figure 3. According to equation (8) the critical value of the cross

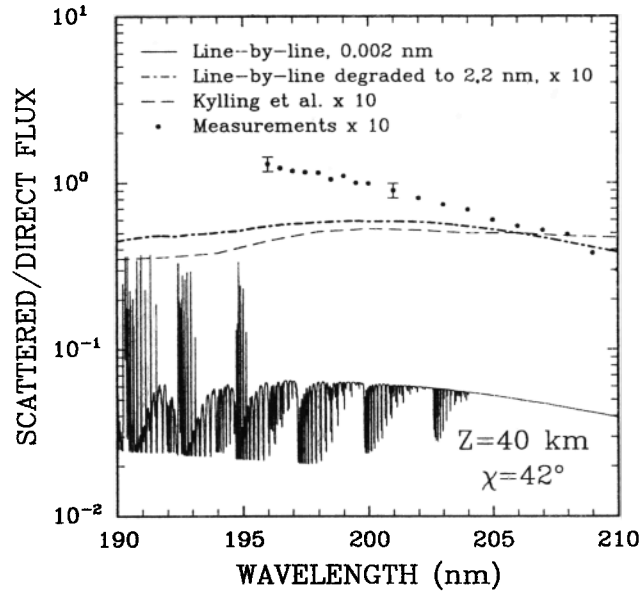

Figure 3. Ratio of scattered to direct fluxes shown at high resolution in Figures 1 and 2 (solid curve). The dash-dot curve shows the flux ratio after both components are spectrally degraded to 2.2 nm. Calculations by *Kylling et al.* [1993] are indicated by the dashed curved. Observed ratio [*Herman and Mentall*, 1982] is shown by the circles, with the ≈10% uncertainty indicated by error bars. All low-resolution ratios have been multiplied by a factor of 10.

section is expected to be smaller at larger solar zenith angles, a result which is verified by the full calculation (equation (1)) for zenith angles greater than 42°.

As discussed earlier, the total scattered flux was determined by *Herman and Mentall* [1982] by integrating the directional radiances over 4π sr, assuming a logarithmic variation between measurements at six viewing angles. In order to define the ratio of scattered to direct flux, they degraded the direct flux measurements to match the 2.2-nm resolution of the scattered flux measurements. The same method is used here to determine the low resolution ratios shown in Figure 3. The *Herman and Mentall* [1982] results and calculations presented by *Kylling et al.* [1993] are also indicated. The new ratios are 20 to 30% larger than values from Kylling et al. below 205 nm, a result which may be attributed to the higher resolution employed here. Nevertheless, the calculation still underpredicts the observed ratio by a factor of 2 to 3 below 200 nm. It should be noted the the twilight effect discussed earlier is concentrated in narrow spectral regions and does not play a significant role in determining the ratio of low resolution fluxes. Clearly, another explanation is required and the following section will address this issue with a detailed analysis of molecular scattering in the 175- to 200-nm wavelength range.

Scattering Cross Sections Below 200 nm

The scattering cross sections used in the above calculations are determined from formulae presented by *Nicolet* [1984], which are based on a fit to the calculations for nitrogen and oxygen by *Bates* [1984]. However, Bates' analysis did not extend below 200 nm and the question may arise whether the scattering cross sections determined from the Nicolet formulae are accurate for these wavelengths. One of the difficulties associated with determining scattering cross sections for air below 200 nm relates to the strong absorption by O_2 in the Schumann-Runge bands. There are limited measurements of the refractive index of oxygen in the Schumann-Runge region [*Smith et al.*, 1976] and no measurements of the depolarization ratio for Rayleigh scattering. Here we briefly outline procedures used to calculate the refractive indices and depolarization ratios for O_2.

The O_2 cross section for Rayleigh scattering at wavenumber ν can be expressed as

$$\sigma_\nu = \left[\frac{32\pi^3\nu^4}{3N_o^2}\right][n_\nu - 1]^2\left[1 + \frac{2}{9}\epsilon_\nu\right] \tag{9}$$

where N_o is Loschmidt's number, n_ν is the real part of the refactive index, and $\epsilon_\nu = |\gamma_\nu/\bar{\alpha}_\nu|^2$. The quantities $\bar{\alpha}_\nu$ and γ_ν represent the mean and anisotropic parts of the polarizability,

$$\bar{\alpha}_\nu = \frac{a_\nu^{\parallel} + 2a_\nu^{\perp}}{3} \tag{10a}$$

$$\gamma_\nu = a_\nu^{\parallel} - a_\nu^{\perp} \tag{10b}$$

where the parallel and perpendicular components of the dynamic polarizability are denoted by $a_\nu^{\parallel}$ and $a_\nu^{\perp}$. The complex refractive index, ξ_ν, is a function of the mean polarizability according to

$$\xi_\nu^2 - 1 = [n_\nu + i\kappa_\nu]^2 - 1 = 4\pi N_o\bar{\alpha}_\nu \tag{11}$$

Finally, the depolarization ratio for Rayleigh scattering [*Young*, 1980] is related to the polarizabilities by

$$\rho_\nu = \frac{6\epsilon_\nu}{45 + 7\epsilon_\nu} \tag{12}$$

The Rayleigh scattering properties are thus completely determined by $a_\nu^{\parallel}$ and $a_\nu^{\perp}$. These quantities are found by summing over all dipole allowed electronic transitions [*Loudon*, 1983],

$$a_\nu^{\parallel} = 3\frac{e^2}{4\pi^2 mc^2}\sum_i \frac{f_i^{\parallel}}{\nu_i^2 - \nu^2 - i\nu\Gamma_i} \tag{13a}$$

$$a_\nu^{\perp} = \frac{3}{2}\frac{e^2}{4\pi^2 mc^2}\sum_j \frac{f_j^{\perp}}{\nu_j^2 - \nu^2 - i\nu\Gamma_j} \tag{13b}$$

where $f_{i,j}$ are the oscillator strengths for transitions i and j; $\nu_{i,j}$ and $\Gamma_{i,j}$ are the associated transition frequencies and absorption line widths. The notation is otherwise standard.

The approach here involves calculation of $a_\nu^{\parallel}$ and $a_\nu^{\perp}$ using a combination of theoretical and experimental results. For the Schumann-Runge transition $X^3\Sigma_g^- \rightarrow B^3\Sigma_u^-$, the measured oscillator strengths and line widths [*Yoshino et al.*, 1983; *Cheung et al.*, 1990] are adopted in conjunction with calculated line positions [*Minschwaner et al.*, 1992]. The band oscillator strengths are normalized using the appropriate Hönl-London factors [*Tatum and Watson*, 1971], assuming a Boltzmann distribution of energies at 250 K. Cross sections for the Schumann-Runge continuum are taken from the measurements by *Ogawa and Ogawa* [1975]. An additional contribution to $a_\nu^{\parallel}$ arising from the transition $X^3\Sigma_g^- \rightarrow B^3\Sigma_u^-$ is estimated based on the results of multiconfigurational time-dependent Hartree-Fock calculations by *Yeager et al.* [1981]. Oscillator strengths and frequencies appearing in equation (13*b*) (primarily $X^3\Sigma_g^- \rightarrow {}^3\Pi_u$ transitions) are obtained also from *Yeager et al.* [1981].

It is important to bear in mind that the polarizabilities are generally complex quantities. The imaginary terms are negligible at frequencies far removed from those associated with electronic transitions [cf. *Dalgarno and Williams*, 1962], but in resonance regions the imaginary parts provide important contributions to both absorption and scattering. For example, the absorption cross section is determined by the imaginary part of the index of refraction according to $\sigma = 4\pi\nu\kappa/N_o$. Both components of the index of refraction are related to the real and imaginary parts of the mean polarizability, $\bar{\alpha}_R$ and $\bar{\alpha}_I$, by equation (11)

$$n^2 - \kappa^2 = 4\pi N_o\bar{\alpha}_R + 1 \tag{14a}$$

$$2n\kappa = 4\pi N_o\bar{\alpha}_I \tag{14b}$$

The calculated refractivity, $n - 1$, is shown in Figure 4 along with measurements by *Smith et al.* [1976]. Differences between the theoretical results and the observations are less than 2%. The refractivity displays irregular variations below about 190 nm due to the influence of Schumann-Runge transitions in vibrational levels above the 5-0 band. As ex-

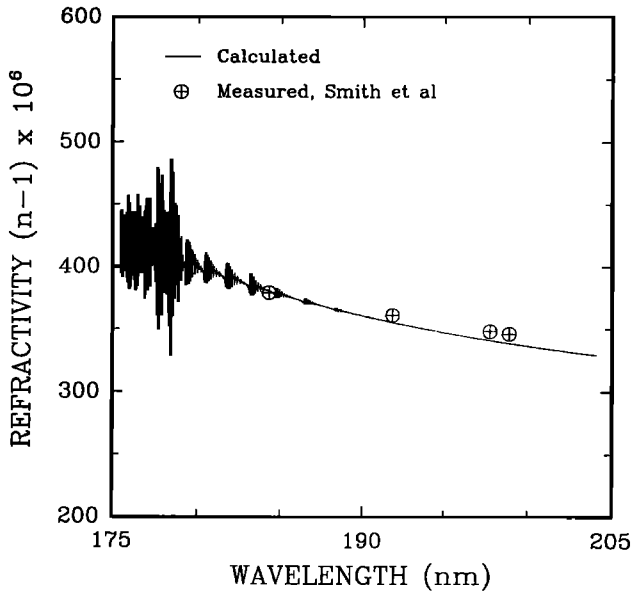

Figure 4. Calculated refractivity of O_2 (solid curve) based on the mean polarizability, as discussed in the text. Circles represent measured refractivity [*Smith et al.*, 1976].

pected on the basis of equations (13*a*) and (13*b*), the refractivity increases abruptly near the long-wavelength approach to strong absorption lines, then decreases on the short-wavelength side in a region characterized by anomalous dispersion ($dn/d\nu < 0$). The same behavior appears in the calculated values of ϵ plotted in Figure 5.

Scattering cross sections for air are shown in Figure 6, determined by the weighted contributions from O_2 according to equation (9) together with the N_2 analysis by *Bates* [1984]. Cross sections based on the *Nicolet* [1984] formulae are also indicated. Differences between the two curves are due to effects of O_2 scattering because the N_2 cross sections are identical in both cases. It is apparent from Figure 6 that the new scattering cross sections will have a negligible impact on the calculated ratio of scattered to direct fluxes between 195 and 205 nm, the spectral region where there is significant discrepancy with the measurements by *Herman and Mentall* [1982]. The revised cross sections are significantly larger below 190 nm, however, particularly near the locations of Schumann-Runge absorption lines.

A further result of the new analysis pertains to the relative intensities of Rayleigh and rotational Raman scattering. *Young* [1982] discusses this issue in detail. Briefly, the cross section described by equation (9) includes contributions from both elastic (frequency unchanged) and inelastic (frequency shifted) scattering. Elastic scattering consists of an isotropic component superimposed on the Q branch of rotational Raman scattering, whereas inelastic scattering is associated with the S branches of Stokes and anti-Stokes Raman lines. The Q and S Raman branches are incoherent, but the isotropic part of elastic scattering is determined by the mean polarizability and corresponds to coherent scattering. The depolarization ratio, as well as ϵ_ν (equation (12)), provides a measure of the relative intensities of these components [*Kattawar et al.*, 1981]. A value of $\epsilon = 1.5$ implies, for example, that about 20% of the scattered radiation is frequency shifted with respect to the incident radiation. Inspection of Figure 5 indicates that ϵ_ν values of this magnitude or larger occur in the Schumann-Runge region; corresponding values of ϵ for N_2 are about 0.19 [*Bates*, 1984], implying that the frequency-shifted components comprise about 5 to 10% of the total scattering by air below 190 nm.

An approximate method has been developed in order to account for these effects in the atmosphere. The approach involves simultaneous solution of the source function at all levels and wavenumbers within a specified spectral interval, as discussed in the appendix. Differences in the scattered to direct flux ratio below 190 nm are on the order of 5 to 10% in the stratosphere compared to the completely elastic approximation using the Nicolet formulae. There is, in addition, a small impact on rates for photolysis of O_2 (1 to 3% larger when considering inelastic scattering). The difference is presumably related to the scattering of available photons from spectral regions between Schumann-Runge absorption features to wavelengths occupied by absorption lines.

Discussion and Conclusion

The observations by *Herman and Mentall* [1982] cannot be explained using a high-resolution treatment of oxygen absorption and refined estimates for Rayleigh scattering. The discrepancy between theory and observation is much larger than the measurement uncertainty reported by *Herman and Mentall* [1982]. The present results suggest that the scattered field below 205 nm arises primarily by single scattering of the direct solar beam; however, calculated direct fluxes are in reasonable agreement with the measurements. Thus the observations, taken at face value, suggest an important omission in the physics contained in theoretical models.

One process neglected here that could affect the scattered field is vibrational Raman scattering. Cross sections in this case are proportional to the derivatives of the polarizabilities.

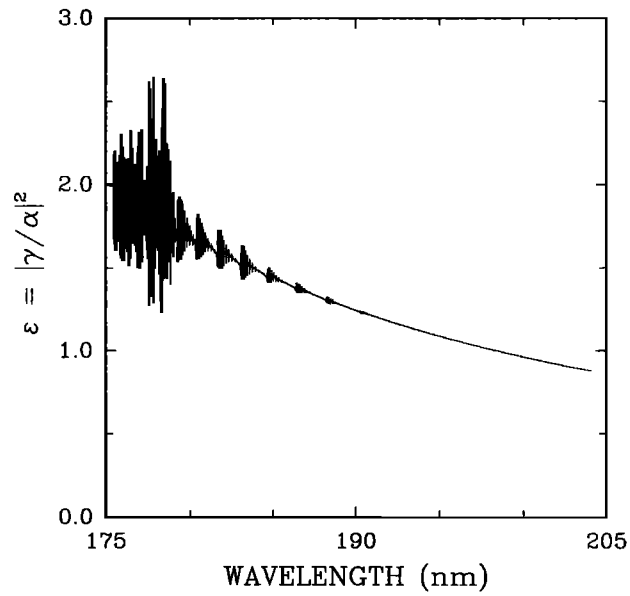

Figure 5. Square of the ratio of anisotropic to mean polarizabilities for O_2, calculated using equations (10*a*) and (10*b*).

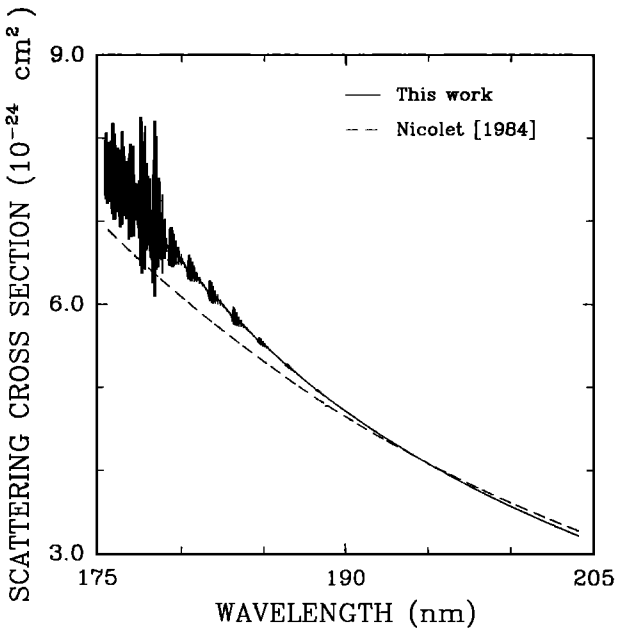

Figure 6. Scattering cross section for air (solid curve) based on calculated O_2 polarizabilities and the N_2 analysis by *Bates* [1984]. The dashed curve shows the scattering cross section determined by the formulae of *Nicolet* [1984].

It may be argued that the importance of this process is small, however, on the grounds that the Stokes ($\nu'' \rightarrow \nu'' + 1$) contribution should dominate over anti-Stokes ($\nu'' + 1 \rightarrow \nu''$) scattering at stratospheric temperatures. This implies that the vibrational Raman component at wavelength λ is determined by scattering of incident radiation at $\lambda - \Delta\lambda$, where $\Delta\lambda$ corresponds to one vibrational quantum (about 9 nm and 6 nm for N_2 and O_2, respectively, at 200 nm). Since the direct solar flux falls off rapidly with decreasing wavelength (Figure 1), it seems unlikely that the inelastic scattering of photons at shorter wavelengths could make a significant contribution to the total scattered field at wavelength λ.

As discussed earlier, the effect of stratospheric aerosols on the scattered flux at 40 km is expected to be small. This assumption is confirmed by the results of additional calculations which included aerosol effects. The treatment of Mie scattering followed the technique developed by *Anderson et al.* [1980], and the vertical profile for extinction was adopted from the extreme volcanic model presented by *Fenn et al.* [1985]. The wavelength dependence of extinction by stratospheric aerosols is small below 550 nm [*Fenn et al.*, 1985], and constant values were employed over the range 190 to 210 nm. The asymmetry parameter was fixed at a value of 0.75 [*Pollack et al.*, 1981]. Differences between these calculations and those which neglect aerosol effects were less than 1% at all wavelengths for altitudes above 35 km, a result which is consistent with the study by *Michelangeli et al.* [1989].

It is of interest, however, to investigate the aerosol extinction required to reproduce the scattered to direct flux ratio near 200 nm observed by *Herman and Mentall* [1982]. The required extinctions are roughly a factor of 100 larger below 40 km as compared to the extreme volcanic model of *Fenn et al.* [1985]; however, the spectral dependence of the ratio is still not adequately simulated. As noted by *Kylling et al.* [1993], the problem in this regard is due to the relatively weak dependence of aerosol optical properties on wavelength. Furthermore, the enhanced levels of extinction (up to 10^{-2} km^{-1}) are unrealistic, particularly for the pre-El Chichon conditions of the 1979 observations by Herman and Mentall [e.g., *Russell et al.*, 1984]. It should be noted that large increases in extinction above 40 km are precluded by the constraints imposed by the direct flux observations.

What appears to be required to explain the observations is a scattering agent concentrated primarily below 45 km, whose scattering efficiency is strongly dependent on wavelength. Further measurements of the direct and scattered radiation field in the stratosphere are required to corroborate the Herman and Mentall results, and to elucidate the processes responsible for determining the direct and scattered radiation fields. Measurement of both quantities at a spectral resolution of 0.1 nm or greater would be particularly valuable.

Appendix: Inelastic Scattering Computations

Rewriting equation (1) to account for inelastic scattering, we have

$$S_\nu(z) = S^o_\nu(z) + \tfrac{1}{2}\int_{z'}\int_{\nu'} S_{\nu'}(z')\sigma_{\nu'-\nu}n(z')E_1\left(|\Delta\tau_\nu|\right)dz'd\nu' \quad \text{(A1)}$$

where $\sigma_{\nu'-\nu}$ represents the cross section for scattering from wavenumber ν' to ν, and $\Delta\tau_\nu$ denotes the extinction optical depth between altitudes z' and z at wavenumber ν. The integration over ν' extends over the spectral range of the rotational Raman lines, which is about 200 cm^{-1} including the Stokes and anti Stokes components [*Weber et al.*, 1967]. Observed line separations are on the order of 11 cm^{-1} for O_2 [*Weber and McGinnis*, 1960] and 8 cm^{-1} for N_2 [*Stoicheff*, 1954]. The ensemble of Raman lines is approximated here by a smooth continuum such that the integrated intensity is consistent with the sum of the Raman line intensities.

The relationships presented by *Kattawar et al.* [1981] between the elastic and inelastic scattering components can be used to express $\sigma_{\nu'-\nu}$ in terms of the total cross section defined by equation (9)

$$\sigma_{\nu'-\nu} = \left(\frac{180 + 13\epsilon_\nu}{180 + 52\epsilon_\nu}\right)\sigma_\nu \quad \text{if } \nu' = \nu \quad \text{(A2a)}$$

$$\sigma_{\nu'-\nu} = \left(\frac{39\epsilon_{\nu'}}{180 + 52\epsilon_{\nu'}}\right)\sigma_{\nu'} \quad \text{if } \nu' \neq \nu \quad \text{(A2b)}$$

where results for a scattering angle of 90° have been applied over all angles. It simplifies the analysis considerably if we assume $\epsilon_{\nu'} \approx \epsilon_\nu$ and $\sigma_{\nu'} \approx \sigma_\nu$. Then equation (A1) reduces to

$$S_\nu(\tau) = S^o_\nu(\tau) + \tfrac{1}{2}\int_{\tau'} E_1\left(|\Delta\tau_\nu|\right)d\tau'_\nu \int_{\nu'} S_{\nu'}(\tau')\Psi(\nu', \nu)d\nu' \quad \text{(A3)}$$

where Ψ is related to the quantities in parentheses in equations (A2*a*) and (A2*b*), representing a normalization factor by which the extinction cross section for scattering (equation 9) must be multiplied in order to obtain the elastic and inelastic scattering contributions.

Equation (A3) can be solved for all values of $S_\nu(\tau)$ using standard matrix inversion techniques. For example, neglecting inelastic scattering, solution of equation (1) involves an $M \times M$ matrix, where M denotes the number of model layers (see the appendix in *Meier et al.* [1982]). For equation (A3), the matrix dimension is $Q \times Q$, where Q is the number of levels times the number of spectral points.

Acknowledgments. I thank Gail Anderson and Al Hall for stimulating discussions which were of great value to this study. Comments on the original manuscript by Sasha Madronich are also appreciated. The research was supported by the Advanced Study Program at the National Center for Atmospheric Research. The National Center for Atmospheric Research is sponsored by the National Science Foundation.

References

Anderson, D. E., R. R. Meier, and J. B. Kumer, Improved model of Mie scattering contribution to tropospheric and stratospheric photodissociation fluxes, *Appl. Opt., 19*, 1230-1231, 1980.

Anderson, G. P., and L. A. Hall, Attenuation of solar irradiance in the stratosphere: Spectrometer measurements between 191 and 207 nm, *J. Geophys. Res., 88*, 6801-6806, 1983.

Anderson, G. P., and L. A. Hall, Stratospheric determination of O_2 cross sections and photodissociation rate coefficients: 191-215 nm, *J. Geophys. Res., 91*, 14,509-14,514, 1986.

Bates, D. R., Rayleigh scattering by air, *Planet. Space Sci., 32*, 785-790, 1984.

Brasseur, G., and S. Solomon, *Aeronomy of the Middle Atmosphere*, D. Reidel, Norwell, Mass., 1984.

Cheung, A. S.-C., K. Yoshino, J. R. Esmond, S. S.-L. Chiu, D. E. Freeman, and W. H. Parkinson, Predissociation line widths of the (1,0)-(12,0) Schumann-Runge absorption bands of O_2 in the wavelength region 179-202 nm, *J. Chem. Phys., 92*, 842-849, 1990.

Dalgarno, A., and D. A. Williams, Raman and Rayleigh scattering of Lyman α by molecular hydrogen, *Monthly Not. R. Astron. Soc., 124*, 313-319, 1962.

Davies, R., Increased transmission of ultraviolet radiation to the surface due to stratospheric scattering, *J. Geophys. Res., 98*, 7251-7253, 1993.

DeMore, W. B., S. P. Sander, D. M. Golden, R. F. Hampson, M. J. Kurylo, C. J. Howard, A. R. Ravishankara, C. E. Kolb, and M. J. Molina, Chemical kinetics and photochemical data for use in stratospheric modeling, Evaluation 10, *JPL Publ. 92-20*, 1992.

Fenn, R. W., S. A. Clough, W. O. Gallery, R. E. Good, F. X. Kneizys, J. D. Mill, L. S. Rothman, E. P. Shettle, and F. E. Volz, Optical and infrared properties of the atmosphere, in *Handbook of Geophysics and the Space Environment*, edited by A. S. Jursa, Air Force Geophysics Laboratory, Bedford, Mass., 1985.

Frederick, J. E., R. D. Hudson, and J. E. Mentall, Stratospheric observations of the attenuated solar irradiance in the Schumann-Runge band absorption region of molecular oxygen, *J. Geophys. Res., 86*, 9885-9890, 1981.

Froidevaux, L., and Yung, Y. L., Radiation and chemistry in the stratosphere: Sensitivity to O_2 absorption cross sections in the Herzberg continuum, *Geophys. Res. Lett., 9*, 854-857, 1982.

Herman, J. R., and J. E. Mentall, The direct and scattered solar flux within the stratosphere, *J. Geophys. Res., 87*, 1319-1330, 1982.

Kattawar, G. W., A. T. Young, and T. J. Humphreys, Inelastic scattering in planetary atmospheres, I, The Ring effect, without aerosols, *Astrophys. J., 243*, 1049-1057, 1981.

Kylling, A., K. Stamnes, R. R. Meier, and D. E. Anderson, The 200- to 300-nm radiation field within the stratosphere: Comparison of models with observation, *J. Geophys. Res., 98*, 2741-2745, 1993.

Lary, D. J., and J. A. Pyle, Diffuse radiation, twilight and photochemistry, II, *J. Atmos. Chem., 13*, 393-406, 1991.

Loudon, R., *The Quantum Theory of Light*, 2nd ed., Oxford University Press, New York, 1983.

Luther, F. M., and R. J. Gelinas, Effect of molecular multiple scattering and surface albedo on atmospheric photodissociation rates, *J. Geophys. Res., 81*, 1125-1132, 1976.

Madronich, S., Photodissociation in the atmosphere, 1, Actinic flux and the effects of ground reflections and clouds, *J. Geophys. Res., 92*, 9740-9752, 1987.

Meier, R. R., D. E. Anderson, and M. Nicolet, Radiation field in the troposphere and stratosphere from 240-1000 nm, I, General analysis, *Planet. Space Sci., 30*, 923-933, 1982.

Michelangeli, D., M. Allen, and Y. L. Yung, The effect of El Chichon volcanic aerosols on the chemistry of the stratosphere through radiative coupling, *J. Geophys. Res., 94*, 18,429-18,443, 1989.

Minschwaner, K., G. P. Anderson, L. A. Hall, and K. Yoshino, Polynomial coefficients for calculating O_2 Schumann-Runge cross sections at 0.5 cm^{-1} resolution, *J. Geophys. Res., 97*, 10,103-10,108, 1992.

Minschwaner, K., R. J. Salawitch, and M. B. McElroy, Absorption of solar radiation by O_2: Implications for O_3 and lifetimes of N_2O, $CFCl_3$, and CF_2Cl_2, *J. Geophys. Res., 98*, 10,543-10,561, 1993.

Nicolet, M., Aeronomic reactions of hydrogen and ozone, in *Mesospheric Models and Related Experiments*, pp. 1-51, edited by G. Fiocco, Springer-Verlag, New York, 1971.

Nicolet, M., On the molecular scattering in the terrestrial atmosphere: An empirical formula for its calculation in the homosphere, *Planet. Space Sci., 32*, 1467-1468, 1984.

Ogawa, S., and M. Ogawa, Absorption cross sections of $O_2(a^1\Delta_g)$ and $O_2(X^3\Sigma_g^-)$ in the region from 1087 to 1700 A, *Can. J. Phys., 53*, 1845-1852, 1975.

Pollack, J. B., O. B. Toon, and D. Wiedman, Radiative properties of the background stratospheric aerosols and implications for perturbed conditions, *Geophys. Res. Lett., 8*, 26-28, 1981.

Rosen, J. M., D. J. Hoffman, and J. Laby, Stratospheric aerosol measurements, II, The worldwide distribution, *J. Atmos. Sci., 32*, 1457-1462, 1975.

Russell, P. B., M. P. McCormick, T. J. Swissler, J. M. Rosen, D. J. Hoffman, and L. R. McMaster, Satellite and correlative measurements of the stratospheric aerosol, III, Comparison of measurements by SAM II, SAGE, dustsondes, filters, impactors, and lidar, *J. Atmos. Sci., 41*, 1791-1800, 1984.

Smith, P. L., M. C. E. Huber, and W. H. Parkinson, Refractivities of H_2, He, O_2, CO, and Kr for $168 \leq \lambda \leq 288$ nm, *Phys. Rev. A, 13*, 1422-1434, 1976.

Stoicheff, B. P., High resolution Raman spectroscopy of gases, *Can. J. Phys., 32*, 630-634, 1954.

Stone, J. M., *Radiation and Optics: An Introduction to the Classical Theory*, McGrawHill, New York, 1963.

Tatum, J. B., and J. K. G. Watson, Rotational line strengths in $^3\Sigma - ^3\Sigma$ transitions with intermediate coupling, *Can. J. Phys., 49*, 2693-2703, 1971.

VanHoosier, M. E., J.-D. F. Bartoe, G. E. Brueckner, and D. K. Prinz, Absolute solar spectral irradiance 120nm-400nm (results from the Solar Ultraviolet Spectral Irradiance Monitor-SUSIM-experiment on board Spacelab 2), *Astro. Lett. Commun., 27*, 163-168, 1988.

Weber, A., and E. A. McGinnis, The Raman spectrum of gaseous oxygen, *J. Molec. Spectrosc., 4*, 195-200, 1960.

Weber, A., S. P. S. Porto, L. E. Cheesman, and J. J. Barrett, High-resolution Raman spectroscopy of gases with cw-laser excitation, *J. Opt. Soc. Am., 57*, 19-28, 1967.

Yeager, D. L., J. Olsen, and P. Jorgensen, The evaluation of MCRPA (MCTDHF) electronic excitation energies, oscillator strengths, and polarizabilities: Application to O_2, *Int. J. Quant. Chem. Quant. Chem. Symp., 15*, 151-162, 1981.

Yoshino, K., D. E. Freeman, J. R. Esmond, and W. H. Parkinson, High resolution absorption cross section measurements and band

oscillator strengths of the (1,0)-(12,0) Schumann-Runge bands of O_2, *Planet. Space Sci., 31*, 339-353, 1983.
Yoshino, K., A. S.-C. Cheung, J. R. Esmond, W. H. Parkinson, D. E. Freeman, and S. L. Guberman, Improved absorption cross sections of oxygen in the wavelength region 205-240 nm of the Herzberg continuum, *Planet. Space Sci., 36*, 1469-1475, 1988.
Young, A. T., Revised depolarization corrections for atmospheric extinction, *Appl. Opt., 19*, 3427-3428, 1980.
Young, A. T., Rayleigh scattering, *Phys. Today, 35*, 42-48, 1982.

K. Minschwaner, Advanced Study Program, National Center for Atmospheric Research, P. O. Box 3000, Boulder, CO 80307

(Received September 10, 1993; revised October 20, 1993; accepted October 21, 1993.)